© 2014. Published by The Company of Biologists Ltd | Development (2014) 141, 4569-4579 doi:10.1242/dev.116103

RESEARCH ARTICLE

An adhesome comprising laminin, dystroglycan and myosin IIA is required during notochord development in *Xenopus laevis*

Nicolas Buisson[1], Cathy Sirour[2], Nicole Moreau[1], Elsa Denker[3], Ronan Le Bouffant[1], Aline Goullancourt[1], Thierry Darribère[1,*] and Valérie Bello[1,*]

ABSTRACT

Dystroglycan (Dg) is a transmembrane receptor for laminin that must be expressed at the right time and place in order to be involved in notochord morphogenesis. The function of Dg was examined in *Xenopus laevis* embryos by knockdown of Dg and overexpression and replacement of the endogenous Dg with a mutated form of the protein. This analysis revealed that Dg is required for correct laminin assembly, for cell polarization during mediolateral intercalation and for proper differentiation of vacuoles. Using mutations in the cytoplasmic domain, we identified two sites that are involved in cell polarization and are required for mediolateral cell intercalation, and a site that is required for vacuolation. Furthermore, using a proteomic analysis, the cytoskeletal non-muscle myosin IIA has been identified for the first time as a molecular link between the Dg-cytoplasmic domain and cortical actin. The data allowed us to identify the adhesome laminin-Dg-myosin IIA as being required to maintain the cortical actin cytoskeleton network during vacuolation, which is crucial to maintain the shape of notochordal cells.

KEY WORDS: Dystroglycan, Notochord, Myosin IIA, Extracellular matrix, *Xenopus laevis*, Cell polarity, Actin

INTRODUCTION

The notochord is the prominent feature of chordates. It is a long, flexible rod that derives from the axial mesoderm and defines the primitive axis of embryos. In *Xenopus laevis*, the notochord is generated through at least four coordinated processes (Keller et al., 1989). First, during gastrulation, notochordal cells that are initially multipolar, acquire stabilizing lamelliform protrusions at the boundary between the notochord and somites, where extracellular molecules – such as laminin, fibronectin, fibrillin and collagen – start to assemble into multimolecular fibrillar complexes. In the second step, from the end of gastrulation to early neurulation, notochordal cells undergo changes in shape. They adopt a spindle-shaped morphology and generate bipolar protrusions to 'tug' on neighboring cells, leading to mediolateral intercalation. These processes cause the lengthening of the notochord. In the next step, occurring from the mid- to late-neurulation stages, cells become flattened and enlarged, transforming the notochord into a cylindrical structure that is surrounded by a fibrous extracellular sheath. In the final step, vacuolation, which begins in cells at the anterior and progesses through to the posterior end of embryos, provides both stiffness and an increase in cell volume, leading to notochord elongation. Vacuoles are lysosome-related organelles that form through a Rab protein and vacuolar-type proton-ATPase-dependent acidification (Ellis et al., 2013). The peri-notochordal sheath, in combination with the turgor pressure exerted by vacuolated cells, provides the rigidity of the notochord that is required for its function as the major skeletal element of embryos. Although the functions of integrin in these mechanisms have already been studied (Davidson et al., 2006), there is no information on the involvement of dystroglycan (Dg; dystroglycan 1, Dag1), the mRNAs of which are present in developing notochord cells (Lunardi and Dante, 2002; Moreau et al., 2003).

Dg is a cell adhesion molecule that links the actin cytoskeleton and the extracellular matrix (ECM) (Ervasti and Campbell, 1993). Dg is encoded by a single gene and cleaved post-translationally into two proteins, resulting in an extracellular glycoprotein, α-Dg, and a transmembrane glycoprotein, β-Dg, which are non-covalently linked to each other (Ibraghimov-Beskrovnaya et al., 1992). α-Dg binds with high affinity to ECM ligands, such as laminin, agrin and perlecan, whereas the cytoplasmic domain of β-Dg binds to cytoplasmic ligands and to signaling proteins (Moore and Winder, 2010).

During embryonic development, laminin-Dg interactions are crucial for early embryonic basement membrane formation. Dg-null mice fail to properly assemble Reichert's membrane, the first extra-embryonic basement membrane, and die early during development (Williamson et al., 1997). In *Xenopus*, Dg plays a key role during the morphogenesis of the pronephros and somites, in laminin assembly and cell anchoring to the basement membrane (Bello et al., 2008; Hidalgo et al., 2009). It also acts as a key signaling component in the Notch pathway during skin differentiation (Sirour et al., 2011).

To uncover the functions of Dg in notochord morphogenesis, we performed knockdown and overexpression experiments, and replaced endogenous Dg with mutated forms of the protein. The findings strongly implicate that Dg acts in an adhesome that is required for laminin assembly, cell polarization during mediolateral intercalation and vacuolation. In addition, for the first time, we identify the non-muscle myosin IIA as a cytoplasmic Dg partner by using immunoprecipitation, mass spectrometry and western blotting. The data show that the adhesome laminin-Dg-myosin IIA is required to maintain the integrity of the cortical actin network during vacuolation.

RESULTS

Dystroglycan depletion affects notochord morphogenesis

The full-length Dg cDNA of *Xenopus laevis* has been previously cloned, and the mRNA expression has been described during early development (Lunardi and Dente, 2002; Moreau et al., 2003). Spatio-temporal analyses of the Dg protein distribution showed that

[1]Sorbonne Universités, UPMC Univ. Paris 06, UMR CNRS 7622, Laboratoire de Biologie du Développement, 75252 Paris, Cedex 05, France. [2]Sorbonne Universités, UPMC Univ. Paris 06, UMR CNRS 7009, Observatoire Océanographique, Villefranche-sur-mer 06230, France. [3]Sars International Centre for Marine Molecular Biology, University of Bergen, Thormøhlensgt. 55, Bergen N-5008, Norway.

*Authors for correspondence (thierry.darribere@upmc.fr; valerie.bello@snv.jussieu.fr)

Received 31 July 2014; Accepted 17 September 2014

Development (2014) 141, 4569-4579 doi:10.1242/dev.116103

it was first detected at the basal poles of dorsal and lateral notochordal cells at the end of gastrulation (stage 13, Fig. 1Aa). Dg then localized to the basal poles of all notochordal cells during neurulation (stage 18, Fig. 1Ab). Although strongly expressed during vacuolation (stages 25-32, Fig. 1Ac,Ad), Dg levels progressively reduced in an anterior to posterior direction towards the end of notochord morphogenesis (stage 37, Fig. 1Ae). This dynamic expression is perfectly correlated with the four processes of notochord morphogenesis and indicates a potential involvement of Dg in these processes.

To address whether Dg is required for correct notochord morphogenesis, we performed knockdown experiments using Dg morpholinos (Dg-MOs). A western blot assay showed a dose-dependent diminution of Dg, with a loss of detection upon use of 33 ng of Dg-MO per embryo (Fig. 1B). Immunofluorescence on cryosections revealed the loss of Dg signals at the basal poles of notochordal cells (Fig. 1Cb). Phenotype analyses of whole embryos showed a dose-dependent shortening of the body axis, which bent dorsally (Fig. 1D). Statistical analysis and the frequencies of phenotypes obtained are summarized in supplementary material Fig. S1.

Phenotypes were examined at the notochord level. A control morpholino (C-MO) or Dg-MO was injected with mRNAs encoding ras that was tagged with green fluorescent protein (ras-GFP); therefore, cells express membrane-bound GFP, allowing visualization of cells containing morpholinos. Cryosections were generated, and the Tor70 antibody, which specifically labels notochord sheath, was used as a marker. C-MO embryos exhibited a fully differentiated notochord that was delineated by the Tor70 labeling. Cells appeared to be correctly positioned, and their vacuoles were inflated (Fig. 1Da). Slight defects were observed in the notochords of embryos that had been injected with 24 ng of Dg-MO (Fig. 1Db); notochord diameters and vacuole sizes were reduced. In embryos that had been treated with 28 ng of Dg-MO, notochord diameters were severely reduced (supplementary material Fig. S5A), vacuoles were absent and Tor70 labeling was discontinuous (Fig. 1Dc, arrowhead). Interestingly, a cell containing the Dg-MO was not integrated into the notochord (Fig. 1Dc, inset, arrows). With 33 ng of Dg-MO, the notochord lacked any recognizable structures (Fig. 1Dd). The Tor70 labeling was undetectable, and isolated cells were scattered in place of the notochord, suggesting a dissociation of the tissue. These phenotypes were fully restored when the Dg-MO and the full-length mRNAs were co-injected (Fig. 1E).

Thus, a dose-dependent knockdown of Dg affects notochord development in a gradual manner, indicating that Dg is required for notochord morphogenesis. In the following experiments, the Dg-MO was injected at 28 ng/embryo.

Dystroglycan is required for laminin deposition in the sheath and notochordal cell recruitment

By the end of gastrulation (stage 13), notochord comprised two or three rows of cells. Dg (Fig. 1Aa) and laminin (Fig. 2Aa) were detected at somite and notochord boundaries. In Dg morphants, notochordal cells were correctly segregated from somites and organized as in controls, but Dg and laminin were absent (Fig. 1Cb, Fig. 2Ab). At early neurulation, the notochord adopted a trapezoidal shape, and laminin was detected at the basal poles of cells (Fig. 2Ac). By contrast, in Dg morphants, the notochord showed a mediolateral enlargement, and laminin was absent (Fig. 2Ad; supplementary material Fig. S5A). Although we could not detect localized signals of laminin in Dg morphants, a western blot

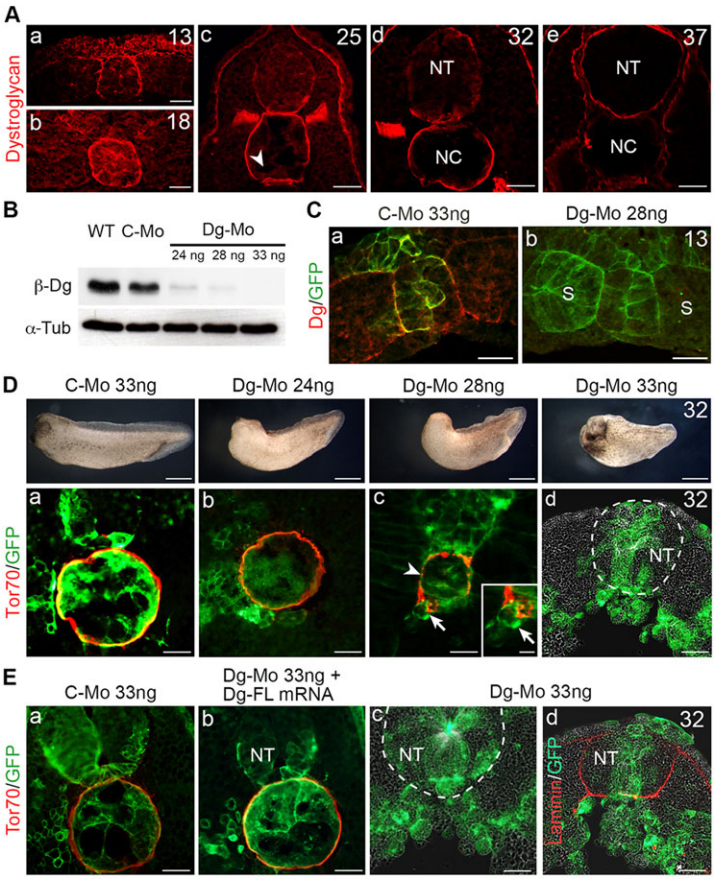

Fig. 1. Dystroglycan depletion affects notochord morphogenesis. (A) Immunodetection of Dg on transverse cryosections from stage 13 to 37 (indicated in the top right of the images). The arrowhead in c indicates a vacuole. (B) Immunoblot of protein extracts from wild-type (WT) embryos or embryos injected with a 5-mispair control morpholino (C-MO) or Dg-MO. (C) Cryosections of embryos co-injected with ras-GFP mRNAs and C-MO (a) or with Dg-MO (b) and then immunostained with antibodies against Dg. In Dg morphants, the Dg staining is lost. (D) The top panels show the embryo phenotypes observed with C-MO or an increasing amount of Dg-MO at stage 32. (a-d) Cryosections treated with Tor70 antibodies showing a dose-dependent effect on the notochord. The arrowhead in c indicates the discontinuity in the notochord sheath. A cell containing Dg-MO (labeled with GFP, arrow and inset in c) escaped from the notochord. (d) At a high amount of Dg-MO, the sheath disappears and the characteristic structure of the notochord is lost. Dotted lines outline the neural tube (NT). (E) Notochord morphogenesis is rescued in Dg morphants through injections of mRNA encoding Dg (Dg-FL mRNA). Dotted lines outline the NT. NC, notochord; S, somite. Scale bars: 25 µm in A,C,Da-d,E; 500 µm in upper panel in D; 10 µm in Dc inset.

Development (2014) 141, 4569-4579 doi:10.1242/dev.116103

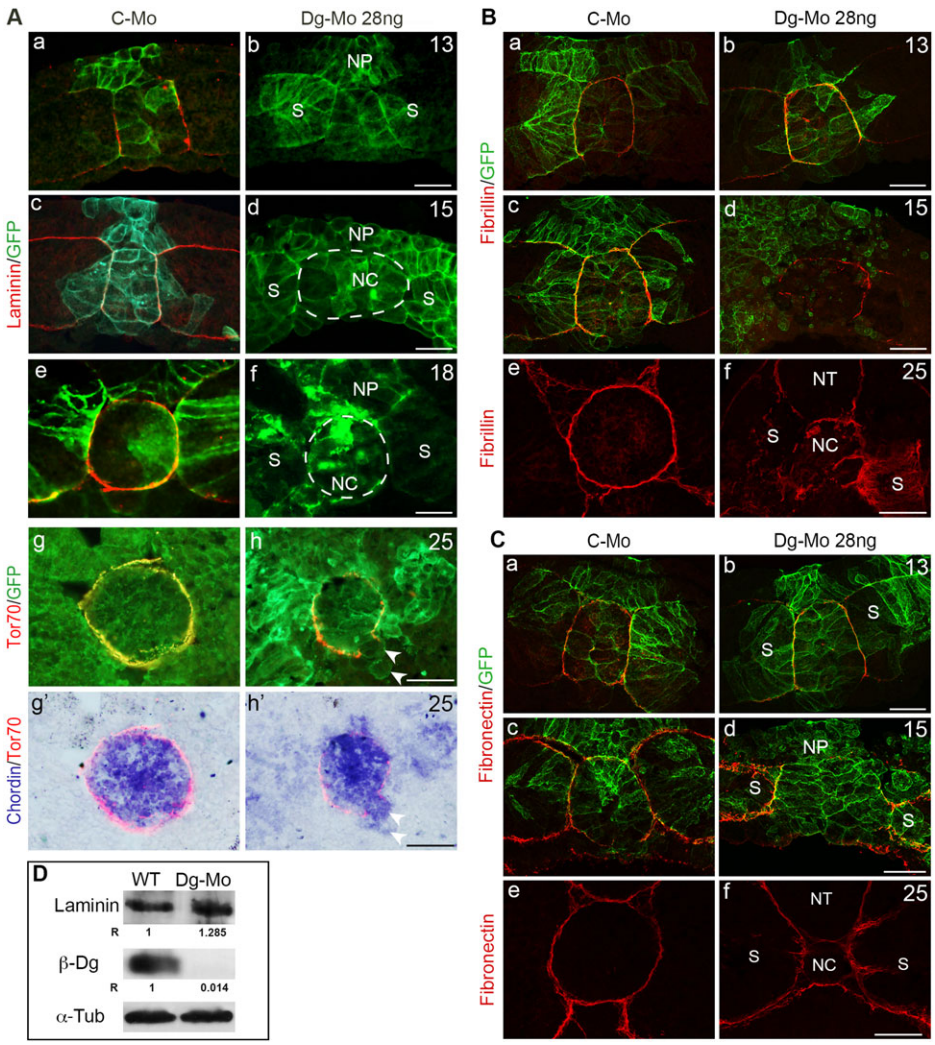

Fig. 2. Dystroglycan depletion affects laminin distribution and notochord morphogenesis. (A) Embryos were co-injected with ras-GFP mRNAs and C-MO or Dg-MO. Immunodetection of laminin or using the Tor70 antibody at stage 13 through to stage 25 (indicated at the top right of the images). (a-h) In Dg morphants, laminin is absent around the notochord (NC). Dotted lines outline the notochord. (g′,h′) *In situ* hybridization for *chordin* and immunodetection using Tor70 were combined at stage 25. Laminin remains absent, and the notochord shape is affected. Arrowheads in h and h′ point to two *chordin*-positive cells (blue in h′) that were depleted of Dg (green in h) and had not integrated in the notochord. (B,C) Embryos were co-injected with ras-GFP mRNAs with C-MO or Dg-MO. Immunodetection of fibrillin (B) and fibronectin (C) at stages 13, 15 and 25. These components of the extracellular matrix are detected in Dg morphants. (D) Immunoblot of protein extracts of wild-type (WT) or Dg-MO embryos (stage 25). In Dg-MO protein extract, Dg is undetected and the amount of laminin is comparable to that of WT. NC, notochord; NP, neural plate; S, somite; R, ratios of laminin and β-Dg to α-tubulin normalized against that of WT are shown under each lane. Scale bars: 25 µm.

analysis revealed that the expression level of laminin was unaffected, indicating that the mRNA expression level was unaffected (Fig. 2D). To ensure that these phenotypes were independent of an effect of Dg-knockdown on cell fates, the distribution of *chordin* transcripts, a specific marker of notochordal cell identity, was examined. At gastrulation, *in toto* analyses revealed an identical spatio-temporal distribution of *chordin* transcripts between controls and Dg morphants (supplementary material Fig. S2). On cryostat sections, laminin was absent around the chordin-positive enlarged notochord of Dg morphants (supplementary material Fig. S3b). We conclude that knockdown of Dg affects notochord morphology without affecting notochord cell fate. At mid-neurulation, the notochord began to round up, and laminin accumulated in the sheath (Fig. 2Ae; supplementary material Fig. S3c). In Dg morphants, notochord morphology was indistinguishable and laminin remained absent (Fig. 2Af; supplementary material Fig. S3d). By stage 25, notochords remained round and were delimited by Tor70 labeling (Fig. 2Ag). In Dg morphants, notochords appeared smaller in sections, laminin was absent (data not shown), and Tor70 labeling was discontinuous (Fig. 2Ah). Interestingly, green-fluorescent cells containing Dg-MO, which were not integrated into the notochord, were positive for *chordin* (Fig. 2Ag′,Ah′, arrowheads). Finally, we also tested whether other ECM components were affected in Dg morphants. Cryosections revealed that fibrillin and fibronectin were correctly expressed in Dg morphants (Fig. 2B,C).

These results establish that, from the mid-neurula stage, Dg is required for laminin deposition around the notochord and suggest that Dg-depleted cells do not participate in notochord morphogenesis.

To fully examine this last phenotype, ras-GFP mRNAs were co-injected with C-MO or Dg-MO in both left blastomeres at the four-cell stage, whereas Rhodamine-lysine dextran (RLDx) alone was injected into the two right blastomeres as an internal control. In controls, C-MO-containing cells and RLDx-marked cells appeared to be involved in notochord formation (Fig. 3A-C,G-I). By contrast, Dg-depleted cells did not contribute to notochord morphogenesis (Fig. 3D-F,J-L). The notochord was formed only by RLDx-marked cells – those that had not received the Dg-MO (Fig. 3L).

Taken together, the results showed that notochordal cell fate was unaltered upon Dg knockdown, whereas the cell surface deposition of laminin did not occur, leading to the breakdown of notochord. The results also show that other constituents of the peri-notochordal sheath, i.e. fibrillin, fibronectin and proteoglycans, that are recognized by Tor70 antibodies were present. Finally, our results show that Dg-depleted cells are excluded from the notochord. These data suggest that laminin-Dg interactions might result in ECM-cytoskeleton linkages or signal-transduction events that are required for notochord morphogenesis.

Development (2014) 141, 4569-4579 doi:10.1242/dev.116103

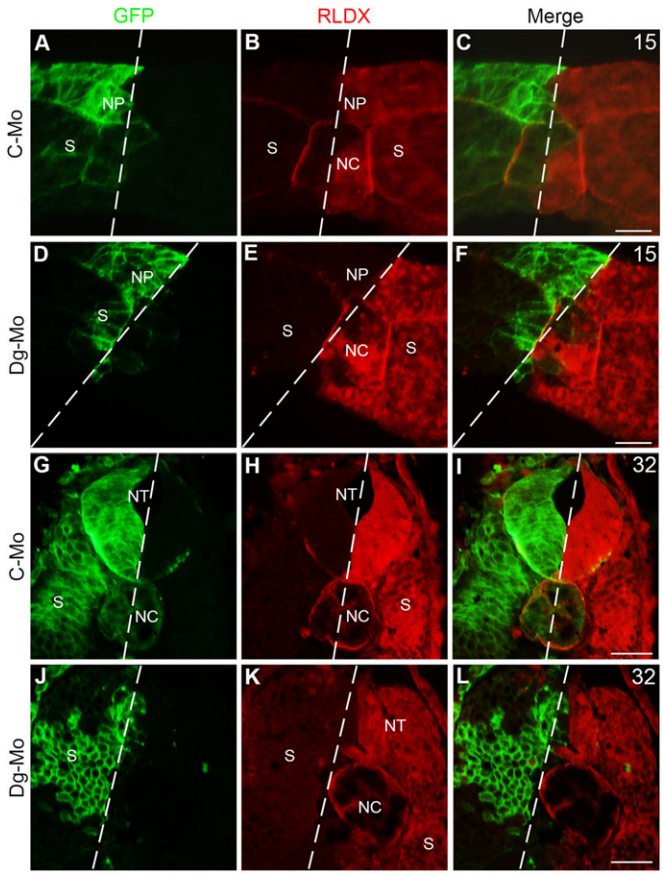

Fig. 3. Dystroglycan-depleted cells failed to integrate into the notochord. At the four-cell stage, the two left blastomeres were injected with C-MO or Dg-MO (33 ng) and ras-GFP mRNAs, the two right blastomeres were injected with RLDx as internal controls. Transverse sections at stages 15 (A-F) and 32 (G-L) are shown. (A-C,G-I) Controls. Notochordal cells containing C-MO (green) or RLDx (red) are implicated equally in notochord formation. The axis of symmetry is indicated by the dotted lines. (D-F,J-L) Dg-MO cells (green) are not integrated into the notochord. NC, notochord; NT, neural tube; S, somite. Scale bars: 25 µm.

The cytoplasmic domain of dystroglycan is needed for notochord morphogenesis

To address the involvement of the Dg cytoplasmic domain downstream of laminin-Dg interactions, notochord morphogenesis was examined in embryos that expressed Dg from which the cytoplasmic domain had been deleted (Dg-Δcyto). Phenotype analyses showed a dose-dependent reduction of the anteroposterior axis, which bent dorsally, as in Dg morphants (Fig. 4A; supplementary material Fig. S4B). At early neurulation, notochordal cells were not correctly organized. Laminin was detected but localized in a dispersed manner on the surface of notochordal cells (Fig. 4Aa,Ab). At stage 32, Tor70 labeling appeared weak and discontinuous around a smaller notochord. Notochord diameters were smaller than controls (supplementary material Fig. S5B). Thus, mutants exhibited slightly different phenotypes to Dg morphants. Laminin was absent in Dg morphants, whereas it was present in mutants, suggesting that laminin binds to Dg mutant proteins on notochordal cell surfaces. However, we cannot rule out that the endogenous Dg is involved in this binding activity. To overcome this possibility, the endogenous Dg was replaced by Dg-Δcyto by using co-injection of Dg-MO (33 ng) with mRNAs encoding Dg-Δcyto. The phenotypes obtained after replacement of Dg by its mutated form were similar to those obtained upon overexpression of Dg mutants (Fig. 4Ac,Ad), indicating that Dg mutant proteins bind to laminin at cell surfaces and that, without the cytoplasmic domain, subsequent notochord development does not occur. These results reinforce the idea that laminin-Dg interactions might act as matrix-cytoskeletal linkages or as platforms for signal transduction events.

The phosphorylation of the cytoplasmic domain is required for vacuolation

There are three known sites in the Dg cytoplasmic domain that interact with cytoplasmic partner proteins (Fig. 4B) (Moore and Winder, 2010). To determine which of these sites is responsible for the above phenotypes, they were mutated. We then performed overexpression experiments or replaced the endogenous Dg with mutants. The efficiency of expression and the amount of mutant proteins produced in the replacement experiments were analyzed for each mutation by western blotting. When the endogenous Dg was replaced, the amount of the Dg mutant proteins produced by embryos was similar to that of endogenous Dg in controls (Fig. 4C).

At its extreme C-terminus, β-Dg comprises the proline-rich motif PPPYVPP, which contains three overlapping motif sequences – PPPY, PYVPP and YVPP. A first construct, Dg-FL PPPY/LALA, was designed to mutate the tyrosine residue that is shared by the three motifs (Fig. 4B). Upon replacement of Dg with the Dg-FL PPPY/LALA mutant, body axes were shorter and abnormally bent, and notochord lengths were shorter than controls (supplementary material Fig. S4B). On sections, no defects were observed by the mid-neurulation stage, and laminin was expressed around the notochord (Fig. 4Da). At the time of vacuolation, vacuoles failed to form, and notochord diameters were strongly reduced (supplementary material Fig. S5B). Notochords were delineated by Tor70 staining (Fig. 4Dd). These phenotypes were slightly different from those of embryos expressing Dg-Δcyto. At neurulation, laminin was present at the basal poles of cells instead of being dispersed on cell surfaces, and morphogenetic disruptions appeared during vacuolation. These observations suggest that the tyrosine residue is required for notochord differentiation.

This tyrosine residue can be phosphorylated (Sotgia et al., 2003). Therefore, to investigate the involvement of phosphorylation in these phenotypes, two additional mutants were constructed: Dg-FL Glu (Y883E) and Dg-FL Phe (Y883F), in which the tyrosine residue was mutated to glutamate and phenylalanine, respectively (Fig. 4B). Expression of the Dg-FL Glu mutant leads to a constitutively phosphorylated motif, whereas the Dg-FL Phe mutation is unable to undergo phosphorylation (Sotgia et al., 2003). No significant differences between controls and the embryos in which Dg had been replaced by Dg-FL Glu were observed at the early and late stages of notochord formation (Fig. 4Db,De; supplementary material Fig. S4B and Fig. S5B). By contrast, the substitution with the Dg-FL Phe mutant revealed similar phenotypes to that of the PPPY/LALA mutants. At neurulation, cells were correctly intercalated, and laminin was observed at the basal poles of cells (Fig. 4Dc). By stage 32, notochord diameters were reduced (supplementary material Fig. S5B), vacuoles were lacking, and the notochord sheaths presented even though they were visibly thinner (Fig. 4Df).

All these results show that phosphorylation of the tyrosine residue in the Dg-cytoplasmic domain is required for notochord morphogenesis. They suggest that laminin-Dg interactions lead to the phosphorylation of the PPPYVPP motif, which is required for the vacuolation of cells.

Development (2014) 141, 4569-4579 doi:10.1242/dev.116103

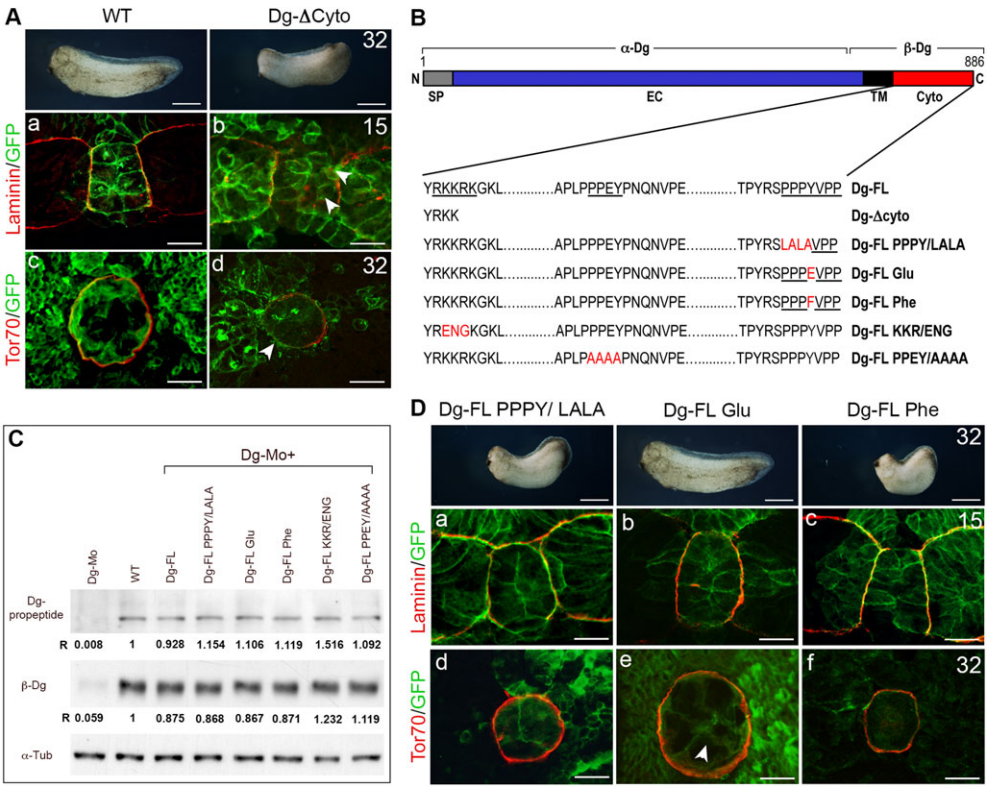

Fig. 4. Dystroglycan mutants lacking the cytoplasmic domain (Dg-Δcyto) and the tyrosine residue of the PPPY motif affect vacuolation. (A) Whole embryos are shown for wild-type (WT) and Dg-Δcyto mutants at stage 32. (a,b) Stage 15 and (c,d) stage 32. Immunodetection of laminin or the Tor70 antibody in controls (a,c), in Dg-Δcyto mutants (b) and in replacement of Dg with Dg-Δcyto mutants (d). In mutants, cells are round instead of exhibiting a fusiform phenotype (b, arrowheads). Laminin is detected. Tor70 staining reveals a discontinuous sheath (d, arrowhead). (B) Schematic representation of Dg cytoplasmic mutants. Dg-Δcyto encodes a protein that does not possess the C-terminus tail. Four amino acids after the transmembrane domain are conserved to ensure that the Dg-Δcyto integrates into the membrane. Dg-FL PPPY/LALA encodes a protein in which the PPPY motif is mutated to LALA. Dg-FL Glu and Dg-FL Phe encode proteins in which the tyrosine residue is mutated to glutamate and phenylalanine, respectively. The Dg-FL KKR/ENG encodes a protein in which the KKR motif is mutated to ENG. The Dg-FL PPEY/AAAA mutant encodes a protein in which the PPEY motif is mutated to AAAA. Underlining indicates consensus binding sequences. (C) Dg-MO was co-injected with mRNAs encoding the Dg mutants. At stage 32, protein lysates were subjected to western blotting using antibodies against β-Dg and α-tubulin. Equivalent amounts of propeptides, endogenous Dg (WT), full-length Dg (Dg-FL) and the mutated β-Dg proteins are observed. R, ratios of Dg-propeptide and β-Dg to α-tubulin normalized to WT. (D) Whole embryos are shown for point mutants at stage 32 in upper panels. Overexpression of Dg-FL PPPY/LALA (a), Dg-FL Glu (b) and Dg-FL Phe (c) proteins on sections at stage 15. Replacement of Dg with Dg-FL PPPY/LALA (d), Dg-FL Glu (e) and Dg-FL Phe (f) on sections at stage 32. Immunodetection of laminin (a-c) and the Tor70 antibody (d-f). The arrowhead in e points to a vacuole. Scale bars: 500 μm in A upper panels, D upper panels; 25 μm in Aa-d,Da-f.

The juxtamembrane and internal sites are needed for mediolateral intercalation of cells

We next investigated the potential function of the binding sequence RKKRK that is localized in the juxtamembrane region of β-Dg (Fig. 4B). Embryos expressing the Dg-FL KKR/ENG mutants, in which the KKR motif is mutated to ENG, showed a reduced trunk length (supplementary material Fig. S4C) and enlarged dorsal structures. By stage 15, the notochord was laterally extended comprising a row of five cells, whereas a row of two cells was observed in controls. Cell shapes appeared rounder than those in controls, suggesting that cells were not polarized (Fig. 5Aa,Ab). The distribution of *chordin* confirmed the lateral extension of the notochord (Fig. 5Ad,Ae). Laminin was present around the notochord and between notochord cells when it should have been present only at the basal poles of cells (Fig. 5Aa,Ab). By stage 32, the mutants showed enlarged notochords with many vacuoles, Tor70 staining was detected around notochords (Fig. 5Ag,Ah; supplementary material Fig. S5C). Counting of Hoechst-stained nuclei showed a substantial increase in enlarged notochord in mutant embryos compared with those of controls (Fig. 5B). This might result either from an increase in cell proliferation or a defect in mediolateral cell intercalation. Cell proliferation, monitored by using a BrdU incorporation assay was analogous between control and mutant embryos (data not shown). To test the second hypothesis, ras-GFP mRNAs alone (control) or Dg-FL KKR/ENG with ras-GFP mRNAs (mutant) were injected into the two left blastomeres of four-cell embryos; RLDx was injected into the right blastomeres of all embryos (Fig. 5C). Frontal sections showed a succession of green and red cells extended across the width of the notochord in controls (Fig. 5Ca). In mutants, a large succession of wild-type cells (marked by RLDx) extended across the notochord, whereas mutant cells (green) did not extend and remained in the left half of the notochord, suggesting a failure to intercalate (Fig. 5Cb).

Next, the function of the PPEY site, located in a more internal position, was examined by a full mutation from PPEY to AAAA (Dg-FL PPEY/AAAA; Fig. 4B). Whole embryo phenotypes of *Xenopus* expressing Dg-FL PPEY/AAAA resembled those obtained with the Dg-FL KKR/ENG mutation: a reduction of anteroposterior axis (supplementary material Fig. S4C) and enlarged dorsal structures. However, they differed at neurulation because the notochord shape resembled that of controls, as indicated by

Development (2014) 141, 4569-4579 doi:10.1242/dev.116103

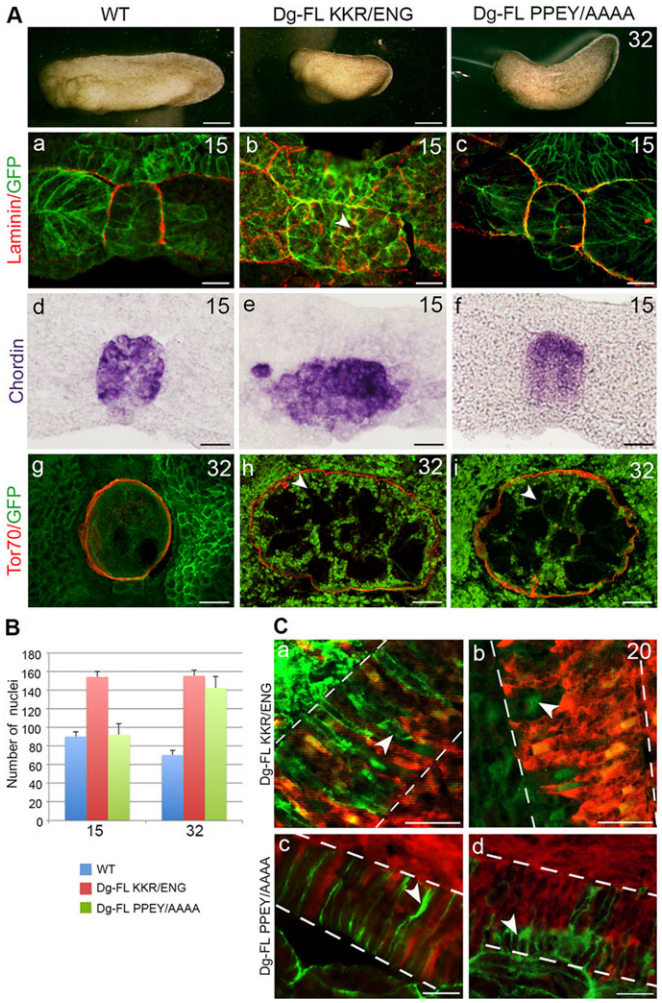

Fig. 5. Mutations in the KKR or PPEY motif result in an enlarged notochord with many vacuoles. (A) Whole embryos are shown for the point mutants at stage 32. Immunodetection of laminin (a-c) and with the Tor70 antibody (g-i) at the stages indicated in the top right. The arrowhead in b points the laminin (red) present around the cell. Arrowheads in h and i indicate numerous vacuoles. (d-f) *In situ* hybridization for the *chordin* gene. (B) Histogram showing the number of Hoechst-stained nuclei in ten transverse sections in the truncal part of wild-type and mutant embryos at stages 15 and 32. Results are means from five independent experiments. (C) Frontal sections of mutants at the level of the notochord. Four-cell-stage embryos were injected with ras-GFP mRNA alone (control; green), or with ras-GFP mRNA and mutant mRNAs into the right blastomeres. RLDx (red) was injected into the left blastomeres. In controls (a,c), red and green cells periodically intercalate and extend along the notochord width (arrowheads in a,c). In mutants, the regular succession of ras-GFP cells (green, arrowheads in b,d) and RLDx cells (red) is lost. Dashed lines outline the notochord. Scale bars: 500 µm in A upper panels; 25 µm in Aa-i,Ca-d.

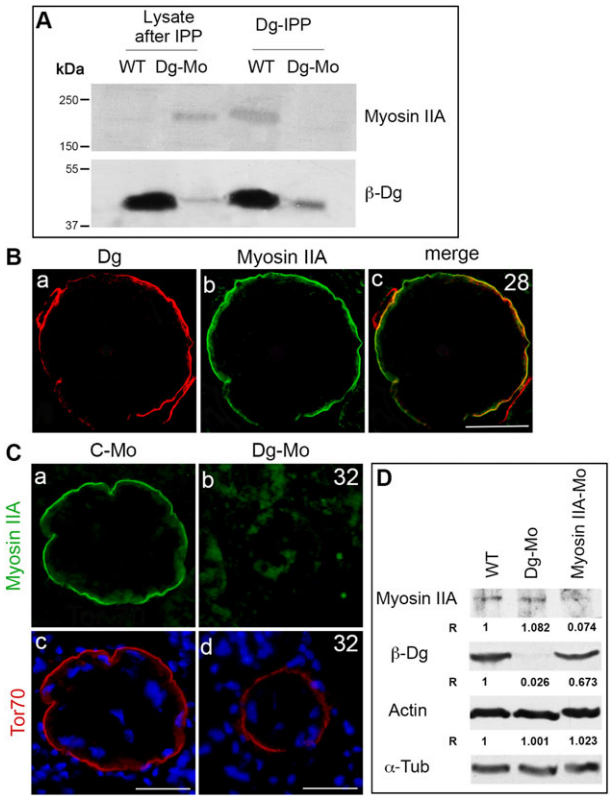

Fig. 6. Myosin IIA is a Dg partner in notochord. (A) Immunoprecipitation (IPP) using an antibody against β-Dg. The precipitate and supernatant of wild-type (WT) and Dg-MO-injected notochords were subjected to western blotting with antibodies against myosin IIA and β-Dg. (B) Identification of Dg and myosin IIA localization using immunofluorescence confocal microscopy. Colocalization of Dg and myosin IIA is observed at cell cortices at stage 28 in WT embryos. (C) Immunodetection of myosin IIA (a,b) and Tor70 proteins (c,d) in C-MO and Dg-MO notochords. Labeling of myosin IIA was lost in Dg morphants at stage 32. Nuclei are stained with Hoechst (blue). (D) Protein extracts of WT, Dg-MO and myosin IIA-MO embryos were subjected to western blotting with antibodies against myosin IIA, actin and α-tubulin (6% SDS-PAGE) and with an antibody against β-Dg (12% SDS-PAGE). In Dg-MO extracts, Dg expression was strongly decreased, whereas the amount of myosin IIA was comparable to that of controls. Note that the decrease in Dg and myosin is not accompanied by a decrease in α-tubulin (α-Tub) or actin. R, ratios of myosin IIA, β-Dg and actin to α-tubulin normalized to WT. Scale bars: 25 µm in B,C.

the distributions of *chordin* and laminin (Fig. 5Ac,Af). By stage 32, an enlarged notochord with many vacuoles was observed (Fig. 5Ai; supplementary material Fig. S5C). The counting of Hoechst-stained nuclei showed a substantial increase compared with controls (Fig. 5B). On frontal sections, Dg-FL PPEY/AAAA notochordal cells did not form a succession of RLDx- and GFP-marked cells. They did not extended across the notochord width and often formed blocks of cohesive cells. These blocks of cells seem to prevent the expansion of wild-type cells through the notochord (Fig. 5Cc,Cd).

All of these results show that juxtamembrane and internal sites are needed for mediolateral cell intercalation. The juxtamembrane site is involved at the beginning of cell intercalation (from stage 15) for correct deposition of laminin. The other sites regulate mediolateral intercalation downstream of laminin deposition. This suggests that they have roles in matrix-cytoskeletal linkages and/or in signaling pathways that are required for cell polarization, which permits mediolateral cell intercalation. Then, we tried to identify partners of cytoplasmic Dg that could mediate Dg function during notochord morphogenesis.

Myosin IIA is a dystroglycan partner required for cytoskeletal integrity

To identify potential cytoplasmic partners of Dg, co-immunoprecipitation reactions coupled to mass spectrometry were performed. To minimize contamination by tissues surrounding the notochord and to increase the amount of protein available, analyses were performed on animal caps that were induced by activin and cultured until they were equivalent to stage 28. To ensure that animal caps containing Dg-MO mimicked phenotypes obtained *in vivo*, the expression of notochord markers Tor70 and *chordin* was

Development (2014) 141, 4569-4579 doi:10.1242/dev.116103

studied in C-MO and Dg-MO caps. The results showed similar phenotypes and expression of markers to those obtained *in vivo* (supplementary material Fig. S6), thereby validating the system used to identify cytoplasmic partners.

Proteins that were immunoprecipitated from lysates of control and Dg-MO caps by using antibodies against β-Dg were identified using tandem mass spectrometry (supplementary material Table S2). Among the identified proteins, myosin IIA was chosen because this protein had a high Mascot score in control cap immunoprecipitates (score 628.7) and, mainly, a null score in immunoprecipitates from Dg-MO caps. Immunoprecipitation and western blotting experiments confirmed the interaction between Dg and myosin IIA. Fig. 6A shows that after immunoprecipitation, myosin IIA was absent from the supernatant of the lysate containing Dg and present in the supernatant of the lysate lacking Dg. It also showed that myosin IIA was present in the immunoprecipitate from the lysate containing Dg and absent in the immunoprecipitate from the lysate lacking Dg. Indirect immunofluorescence showed that myosin IIA was barely detectable in notochord at stage 18, clearly visible at stage 23 and colocalized with Dg in the apical cortex of notochordal cells (Fig. 6B). Altogether, these results suggest that Dg and myosin IIA are associated in complexes at cell cortices.

To further investigate this finding *in vivo*, the distribution of Dg and myosin IIA was examined in morphants. In Dg morphants, the immunolabeling of myosin IIA was lost (Fig. 6Ca,Cb) but not that by the Tor70 antibody, as expected (Fig. 6Cc,Cd). Likewise, the amount of myosin IIA, actin and α-tubulin was similar to that of control (Fig. 6D), suggesting that the localization of myosin IIA to notochordal cell cortices is dependent on Dg proteins.

To further probe the role of myosin IIA, loss-of-function experiments using morpholinos against myosin IIA (myosin IIA-MO) were performed. The efficiency of the myosin IIA-MO was assessed by using a western blotting and immunofluorescence assays, showing the absence of the protein (Fig. 7A,B). Myosin-morphants exhibited enlarged dorsal structures and a reduction of the anteroposterior axis. On sections, the notochord was strongly enlarged (supplementary material Fig. S5D). Dg, laminin and Tor70 staining was immunodetected around the notochord, and interestingly Dg and laminin were present between cells (Fig. 7Ca-f). The detection of the ras-GFP protein highlighted the increasing size of vacuoles of myosin IIA-depleted cells (Fig. 7Ce,Cf).

Knowing the role of myosin IIA in the actin cytoskeleton organization (Conti and Adelstein, 2008), we questioned whether depletion of myosin IIA affects the integrity of the actin and microtubule cytoskeletons. In controls, detection of F-actin by using phalloidin showed a dense actin network in the cortices of notochordal cells (Fig. 7Da,Dd). By contrast, a strong reduction in F-actin staining was observed in myosin morphants (Fig. 7Db; supplementary material Fig. S7). Few actin filaments were detected in cortices, indicating that the establishment of cortical actin networks requires myosin IIA (Fig. 7Dd,De). Unexpectedly, the dense microtubule network that was labeled with antibodies against tubulin and extended towards the center of control cells (Fig. 7Dg, Dj) was lost in myosin morphants (Fig. 7Dh,Dk). The majority of microtubules formed thick bundles that were packed against cell membranes (Fig. 7Dh,Dk). The distribution of actin filaments and microtubules was also studied in the absence of Dg. Actin (Fig. 7Dc,Df) and microtubule (Fig. 7Di,Dl) networks were strongly affected, as seen in myosin morphants. It is noteworthy that in Dg and myosin morphants, the amount of actin and α-tubulin did not change substantially (Fig. 6D, Fig. 7A).

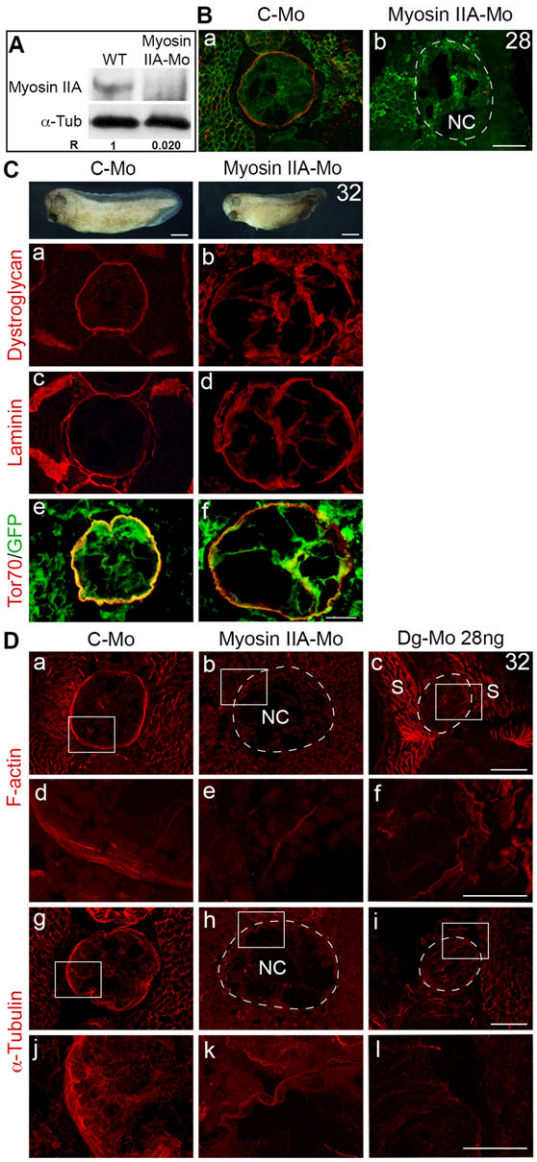

Fig. 7. Myosin IIA is required for cytoskeletal integrity. (A) Protein extracts of wild-type (WT) or myosin IIA-MO embryos were subjected to western blotting with antibodies against myosin IIA and α-tubulin, which showed the efficiency of the morpholinos. R, ratios of myosin IIA to α-tubulin normalized to WT. (B) Immunodetection of myosin IIA in C-MO and myosin IIA-MO notochords. Labeling of myosin IIA was lost in morphants at stage 28. Dotted lines outline the notochord (NC). (C) Phenotypes of control and myosin IIA morphants at stage 32. (a-d) Immunodetection of Dg and laminin in C-MO embryos and morphants. The notochord diameter and the vacuole size increased. Myosin IIA depletion does not affect Dg and laminin expression, but they do not localize normally. (e,f) Tor70 labeling confirms the increase in the size of the notochord and vacuoles. (D) F-actin and α-tubulin localization, by using confocal microscopy, in control and myosin IIA- and Dg-depleted notochord at stage 32. (a-f) F-actin is revealed by staining with phalloidin. (d-f) Magnification at the cell cortex showing the loss of labeling in morphants; the area corresponds to that highlighted by the white box in the panel above. (g-l) Tubulin is revealed by using an antibody against α-tubulin. (j-l) Magnification at the cell cortex showing the network disruption of α-tubulin; the area corresponds to that highlighted by the white box in the panel above. Dotted lines outline the notochord. S, somite. Scale bars: 25 μm in B,Ca-f,Da-c, Dg-i; 500 μm in C upper panels; 10 μm in Dd-f,Dj-l.

These results show that myosin IIA and Dg are colocalized in the cortices of notochordal cells and that ablation of Dg abolishes the cortical localization of myosin IIA. They show that ablation of

Development (2014) 141, 4569-4579 doi:10.1242/dev.116103

non-muscle myosin IIA leads to the localization of Dg and laminin at the whole-cell surface when they should be located at the basal pole of cells. Finally, the myosin IIA and Dg ablation also leads to disruption of F-actin and α-tubulin. Overall, the results show that laminin, Dg, myosin IIA, F-actin and tubulin are required for notochord morphogenesis.

DISCUSSION

In this work, we provide *in vivo* functional data on the involvement of Dg in notochord morphogenesis. Using Dg depletion, overexpression of Dg cytoplasmic mutants and replacement of endogenous Dg by mutants, three major phenotypes were identified: the absence of laminin binding to the cell surface, leading to the breakdown of notochord; an impairment of cell polarity leading to disruption of mediolateral intercalation; and a deficiency in vacuole formation, leading to the reduction of the diameter and length of the notochord.

The depletion of Dg and the deletion of the β-Dg cytoplasmic domain gave rise to comparable phenotypes, except that laminin was associated with cell surfaces in cytoplasmic mutants, whereas it was absent in Dg morphants. In both cases, the notochord failed to form, suggesting that Dg is required for laminin deposition in the notochord sheath and that laminin-Dg interactions might act as matrix-cytoskeletal linkages or as a platform for signal-transduction events that are required for notochord morphogenesis. It is known that fibronectin and fibrillin are components of the notochordal sheath that appears during gastrulation. At somite-notochord boundaries, fibrillin regulates the convergence and extension of mesodermal cells, leading to the segregation of notochordal cells and to the trapezoidal shape of the notochord (Skoglund et al., 2006; Skoglund and Keller, 2007). Fibronectin fibrils are required for epiboly but not convergence and extension (Rozario et al., 2009). We show that fibrillin and fibronectin were expressed around the trapezoidal notochord. Later, their expression was maintained, and if depositions of fibronectin and fibrillin appeared to be affected around the notochord in Dg morphants, this is because of the defective architecture of the notochord, not a loss of these proteins. Therefore, our data do not support a role for these molecules in the observed notochord phenotypes, rather, they suggest that fibrillin and fibronectin deposition in the ECM starts earlier than the expression of Dg and that their assembly into fibrils can occur independently of Dg. In zebrafish, knockdown using a Dg-MO has a significant effect only on myogenesis, whereas an essential role for laminins in notochord formation has been shown (Parsons et al., 2002a,b). This suggests a redundancy with other extracellular matrix receptors for notochord morphogenesis in zebrafish, which does not seem to be the case in *Xenopus*, according to our results. These differences highlight that Dg functions seem to vary according to species, tissues and organs, and especially during embryonic development (Bello et al., 2014).

An impairment of cell polarity leading to disruption of mediolateral intercalation is observed with the KKR/ENG and PPEY/AAAA mutants. Mutation of the RKK/ENG domain, as done previously by Spence and colleagues (Spence et al., 2004), leads to a broadening of the notochord with a deposition of laminin around the notochord and, unexpectedly, between cells at an earlier stage. At later stages, a peri-notochordal sheath surrounded an enlarged notochord comprising numerous small vacuoles, suggesting that notochord differentiation was unaffected. The RKKRK sequence is known to bind to ezrin-radixin-moesin (ERM) proteins and ERK/MAP kinases and confers to Dg a role in the formation of actin-rich membrane protrusions, such as filopodia-like structures (Batchelor et al., 2007). Dg was shown to function as a scaffold for components of the actin-signaling machinery that, independently of out-in signaling, leads to the localized activation of Cdc42, which is implicated in filopodia formation via a ternary complex of Dg, ezrin and elements of the Rho GTPase signaling (Batchelor et al., 2007). In view of the data, it is likely that cell mediolateral intercalation defects are related to a failure of actin cytoskeleton rearrangement, leading to cell polarity defects. Because ezrin is not expressed in the notochord (N.B. and V.B., unpublished), several scenarios are possible. First, other unidentified adaptor proteins might interact with Dg to mediate the activation of a signaling pathway involved in cytoskeleton remodeling. Another possibility is that the mutant could interfere with the Wnt-planar cell polarity (PCP) pathway. Data supporting this hypothesis is that laminin and Dg were distributed across the whole periphery of cells, instead of being distributed only to the basal poles of cells. This phenotype resembles that described in *Ciona* mutants, for which the Prickle component of the Wnt-PCP pathway was mutated (Veeman et al., 2008). The PCP proteins Prickle, Strabismus and Dishevelled have been shown to be important in restricting fibronectin localization to the outer surfaces of notochordal cells (Goto et al., 2005). It is possible that similar mechanisms are employed for the localization of laminin and Dg in KKR/ENG mutants. Unlike in KKR/ENG mutants, intercalation occurred in PPEY/AAAA mutants during early neurulation, but then cell intercalation was perturbed and the notochord became much wider after neurulation, as in KKR/ENG mutants. This difference in timing of the phenotype onset could be explained by a functional redundancy between the two WW-binding motifs. It has been shown that the WW-binding motifs of the internal and terminal sequences of Dg are both able to bind to dystrophin *in vivo* and are involved in the establishment of cell polarity in *Drosophila* (Yatsenko et al., 2009). It is therefore possible that KKR sites are required for early intercalation and then the PPEY site is used. Further studies will be needed to show whether their activities are regulated during notochordal cell intercalation.

A deficiency in vacuole formation is established when the extreme C-terminal domain of β-Dg is mutated. It contains the motif PPPYVPP, which is known to have three overlapping binding domains: WW, SH3 and SH2. We find that the PPPY motif, a SH2-binding domain, is required for vacuolation that depends on its phosphorylation. During neurulation, cells are correctly intercalated, but subsequently vacuoles fail to form. It is known that Dg engagement by laminin generates a phosphotyrosine signal leading to the interaction of its cytoplasmic domain with signaling molecules (Ilsley et al., 2001; Sotgia et al., 2001). It is therefore likely that the phosphorylation of the tyrosine residue leads to interactions with components of a signaling pathway that is involved in vacuolation processes.

A proteomic analysis was performed to identify β-Dg-specific partners involved in notochord morphogenesis. One identified ligand was myosin IIA, which is expressed in the notochord. It belongs to the non-muscle myosin class II family. In vertebrates, there are three isoforms, MHC-A, MHC-B and MHC-C, which have enzymatic and structural roles in cell polarity, cell migration and cell adhesion (Vicente-Manzanares et al., 2009). In *Xenopus*, the role of myosin IIB has been studied in the notochord and neural tube (Skoglund et al., 2008; Rolo et al., 2009). Myosin IIB participates in the morphogenesis of these two tissues by organizing a polarized cortical actin network that is required for cell polarity and regulation of cell adhesion. We show that myosin IIA is detected in the notochord after mediolateral cell intercalation (stage 23), where it colocalizes with Dg. Interestingly, Dg is essential for the correct targeting of myosin IIA to membranes. Myosin IIA morphants

Development (2014) 141, 4569-4579 doi:10.1242/dev.116103

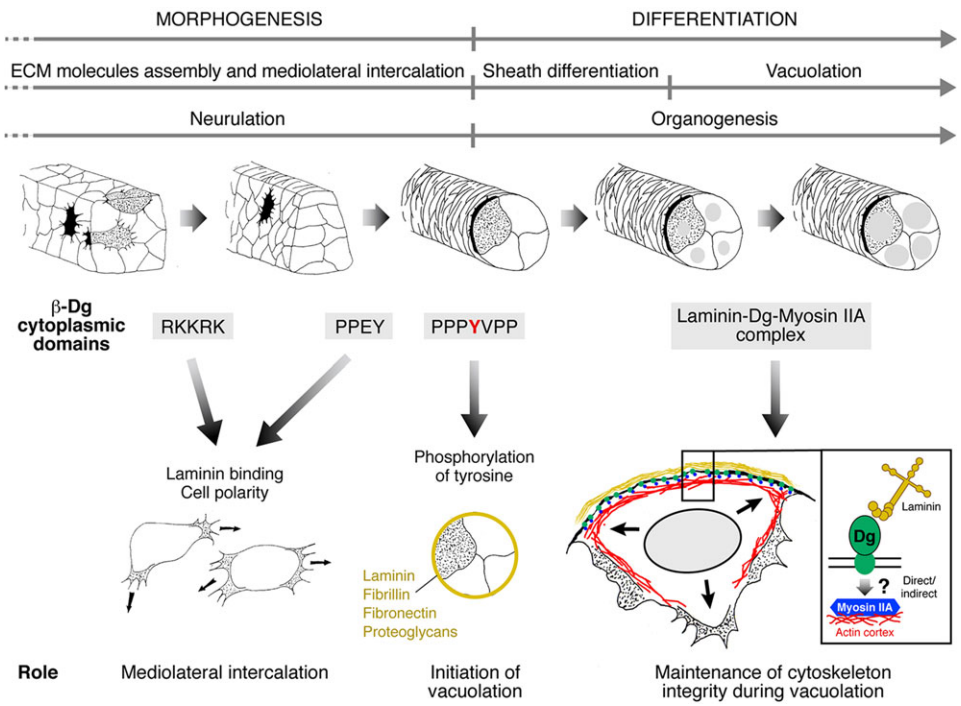

Fig. 8. The Dg adhesome is involved throughout notochord morphogenesis. The data have established that, when Dg binds to laminin, the RKKRK and PPEY sites of the cytoplasmic domain are mobilized to ensure cell polarity and mediolateral intercalation. Laminin-Dg interactions lead to phosphorylation of the tyrosine residue in the PPPYVPP site to generate a signaling pathway that allows vacuole differentiation. Finally, an adhesome comprising laminin-Dg-myosin-IIA-actin is established to maintain cortical integrity during vacuolation. The sheath is shown in yellow. (Adapted from Keller et al., 1989.)

exhibited an enlarged notochord with a loss of cell shape, suggesting a role in the regulation of cell polarity and cell shape, and therefore maintenance of cytoskeleton integrity. Effectively, the study of actin and microtubule networks in myosin IIA-depleted cells show that both networks are affected. It is possible that a perturbation of the actin network can be transmitted to the microtubule network, leading to a strong disorganization of the cytoskeleton as it has been demonstrated previously for growth cone guidance, cell division, wound healing and cortical flow (Rodriguez et al., 2003).

The loss of cell shape observed in myosin IIA morphants begins at stage 25, which coincides with the strong presence of myosin IIA in the notochord and at the beginning of vacuolation. These observations suggest that myosin IIA behaves as an actin filament cross-linker to control the cortical integrity and to contribute stiffness to cells. These characteristics are essential for notochordal cells to resist to the stretching induced by the strong pressure increase in vacuoles. It has been shown that myosin IIB controls actin dynamics during cell-cell and cell-ECM interactions that are required for mediolateral intercalation during early notochord formation (Skoglund et al., 2008). Here, we show that myosin IIA, localized exclusively in cell cortices at the level of cell-ECM contacts, controls actin dynamics during late notochord differentiation.

We propose that Dg is required throughout notochord morphogenesis (Fig. 8). During gastrulation, fibrillin deposition at the somite-notochord boundaries occurs until stage 13, initiating the convergence and extension of axial mesodermal cells which segregates cells from somites and gives rise to the trapezoidal shape of the notochord (Skoglund et al., 2006; Skoglund and Keller, 2007). Then, Dg begins to be expressed and its binding to laminin mobilizes the RKKRK and PPEY sites of the cytoplasmic domain in order to strengthen cell polarity and mediolateral intercalation. Next, laminin-Dg interactions lead to the phosphorylation of the tyrosine residue in the PPPYVPP site which might generate a signaling pathway that promotes vacuolation. Finally, an adhesome comprising laminin, Dg, myosin IIA and actin is established in order to maintain cortical cytoskeletal integrity during vacuolation processes.

MATERIALS AND METHODS

Xenopus embryos and microinjections

Xenopus laevis embryos were obtained using standard methods and staged according to Nieuwkoop and Faber (Nieuwkoop and Faber, 1994). The Dg morpholino (Dg-MO) and the mismatch Dg morpholino (C-MO) have been described previously (Hidalgo et al., 2009). The sequence of the myosin IIA morpholino was: 5′-ACTTGTCCACATCTGTTTGTGCCAT-3′ (Gene Tools). For controls of myosin IIA morpholino injections, the Gene Tools standard control morpholino was used. Morpholinos were injected into either both left blastomeres at the four-cell stages (14 ng/blastomere) or into the four dorsal blastomeres at the eight-cell stages (7 ng/blastomere). Morpholinos were injected with ras-GFP mRNAs as a lineage tracer (320 pg/blastomere at the four-cell stage or 140 pg/blastomere at the eight-cell stage).

Plasmid constructs and mRNA injection experiments

The construction deleted of the β-Dg cytoplasmic domain (Dg-Δcyto) has been described previously (Bello et al., 2008). Dg was cloned into the pCS2+ vector between *Bam*HI and *Cla*I restriction sites, and point mutations were performed using the QuikChange Site-directed Mutagenesis kit (Stratagene) according to the manufacturer's instructions and using the primers listed in supplementary material Table S1. Synthetic capped mRNAs were generated through *in vitro* transcription as described previously (Djiane et al., 2000). Embryos were injected at the eight-cell stage into the four dorsal blastomeres (317 pg/blastomere) to target notochordal cell progenitors.

In situ hybridization and immunodetection

Whole-mount *in situ* hybridization analyses were performed as described elsewhere (Harland, 1991). Immunostaining of frozen sections was performed as described previously (Bello et al., 2008). For immunodetection of myosin IIA, embryos were treated with Dent's fixative. The antibodies used were: mouse anti-β-dystroglycan (43DAG/8D5, Novacastra, 1:50), rabbit anti-α-l-laminin (L-9393, Sigma-Aldrich, 1:100), mouse anti-GFP (1814460, Roche, 1:400), rabbit anti-GFP (ab290, Abcam, 1:250), mouse anti-proteoglycans Tor70 (Florence Broders, Curie Institute, Paris, France), rabbit anti-myosin-IIA (M8064, Sigma-Aldrich, 1:100), mouse anti-fibronectin (4H2; Douglas

Development (2014) 141, 4569-4579 doi:10.1242/dev.116103

DeSimone, University of Virginia, Charlottesville, VA; 1:100), mouse anti-fibrillin (JB3, Hybridoma bank, 1:50), Alexa 568 phalloidin (A12380, Invitrogen, 1:1000), mouse anti-α-tubulin (T9026, Sigma-Aldrich, 1:1000). Nuclei were stained with Hoechst (H33258, Sigma-Aldrich, 1:1000).

BrdU incorporation

Cell proliferation was detected with 5-bromo-2′deoxyuridine (Hardcastle and Papalopulu, 2000). At stages 13, 15 and 17, 10 nl BrdU (Roche) was injected bilaterally into the archenteron. Embryos were fixed 1 h later in MEMFA. Cryostat sections were then subjected to immunostaining for BrdU (347580, Becton Dickinson, 1:200).

Western blotting

Lysates from embryos or immunoprecipitates were separated by using 6% or 12% SDS-PAGE and then transferred to nitrocellulose membrane as described previously (Sirour et al., 2011). The antibodies used were: mouse anti-β-Dg (43DAG/8D5, Novacastra, 1:100), rabbit anti-α-l-laminin (L-9393, Sigma-Aldrich, 1:100), rabbit anti-non muscle myosin IIA (M8064, Sigma-Aldrich, 1:100), mouse anti-α-tubulin (T9026, Sigma-Aldrich, 1:10,000), goat anti-actin (sc-1616, Santa Cruz, 1:500). Data are representative of three independent experiments. Blots were quantified using ImageJ software. For each immunoblot, the normalized ratios of proteins to α-tubulin are shown.

In vitro induction of notochord

Embryos were injected into both blastomeres at the two-cell stage with Dg-MO (14 ng for immunochemistry and 16.5 ng for immunoprecipitation analyses). Animal caps were then isolated from the control and injected embryos at stage 8, immersed for 1 h (equivalent to stage 10.5) in 1×MBS 0.1% BSA containing activin A (A4941, Sigma-Aldrich, 80 ng/ml) and transferred to 1×MBS until the caps were equivalent to stage 28 of development (Ariizumi and Asashima, 2001).

Immunoprecipitation

Notochord explants (n=500) or stage 28 embryos (n=100) were lysed in lysis buffer (1% Triton X-100, 150 mM NaCl, pH 7.5, 10 mM Tris, 1 mM EDTA, 1 mM EGTA, 0.5% NP-40, 0.2 mM PMSF) with protease inhibitors. After centrifugation, the supernatant was used for immunoprecipitation using Dynabeads M-280 sheep anti-rabbit IgG (Invitrogen, 112.03D). Magnetic beads (20 µl) were incubated for 2 h with 2 µg rabbit anti-β-Dg antibody (sc-28535, Santa Cruz) and treated according to the manufacturer's instructions.

Tandem mass spectrometry

Immunoprecipitated proteins were digested directly on the beads overnight at 37°C by using sequencing grade trypsin (12.5 µg/ml, Promega) in 20 µl of 25 mM NH_4HCO_3. Digests were analyzed by using an LTQ Velos Orbitrap (Thermo Fisher Scientific) coupled to an Easy nano-LC Proxeon system (Thermo Fisher Scientific) as described previously (Philippe et al., 2013). MS-MS data were searched against SwissProt databases using the *Xenopus laevis* and *Xenopus tropicalis* taxonomies. Proteins with a Mascot score higher than 45 and a null score in the Dg-MO immunoprecipitates were considered as putative Dg partners. Mascot scores are the means±s.e.m. from three different experiments.

Acknowledgements

We thank M. Umbhauer and J. F. Riou for helpful comments; M. A. Conti for kindly providing antibodies against myosin IIA and myosin IIB; P. Skoglund for technical advice about myosin IIA; T. Leger of the Mass Spectrometry Facility (Jacques Monod Institute, University Paris-Diderot, France); R. Schwartzmann for confocal imaging; S. Gournet for photographic assistance; and S. Autier for animal care.

Competing interests

The authors declare no competing financial interests.

Author contributions

N.B. and V.B. performed the experiments with assistance from C.S., N.M., E.D., R.LeB. and A.G.; T.D. and V.B. designed the experiments, analyzed results and wrote the manuscript.

Funding

This work was supported by the Centre National de la Recherche Scientifique (CNRS) and Université Pierre et Marie Curie (UPMC). N.B. was supported by a doctoral fellowship from the Regional Council of Martinique, BRFD (Bourse Régionale de Formation Doctorale).

Supplementary material

Supplementary material available online at
http://dev.biologists.org/lookup/suppl/doi:10.1242/dev.116103/-/DC1

References

Ariizumi, T. and Asashima, M. (2001). *In vitro* induction systems for analyses of amphibian organogenesis and body patterning. *Int. J. Dev. Biol.* **45**, 273-279.

Batchelor, C. L., Higginson, J. R., Chen, Y.-J., Vanni, C., Eva, A. and Winder, S. J. (2007). Recruitment of Dbl by ezrin and dystroglycan drives membrane proximal Cdc42 activation and filopodia formation. *Cell Cycle* **6**, 353-363.

Bello, V., Sirour, C., Moreau, N., Denker, E. and Darribère, T. (2008). A function for dystroglycan in pronephros development in *Xenopus laevis*. *Dev. Biol.* **317**, 106-120.

Bello, V., Moreau, N., Sirour, C., Hidalgo, M., Buisson, N. and Darribère, T. (2014). The dystroglycan: nestled in an adhesome during embryonic development. *Dev. Biol*. (in press).

Conti, M. A. and Adelstein, R. S. (2008). Nonmuscle myosin II moves in new directions. *J. Cell Sci.* **121**, 11-18.

Davidson, L. A., Marsden, M., Keller, R. and DeSimone, D. W. (2006). Integrin alpha5beta1 and fibronectin regulate polarized cell protrusions required for Xenopus convergence and extension. *Curr. Biol.* **16**, 833-844.

Djiane, A., Riou, J., Umbhauer, M., Boucaut, J. and Shi, D. (2000). Role of frizzled 7 in the regulation of convergent extension movements during gastrulation in *Xenopus laevis*. *Development* **127**, 3091-3100.

Ellis, K., Bagwell, J. and Bagnat, M. (2013). Notochord vacuoles are lysosome-related organelles that function in axis and spine morphogenesis. *J. Cell Biol.* **200**, 667-679.

Ervasti, J. M. and Campbell, K. P. (1993). Dystrophin-associated glycoproteins: their possible roles in the pathogenesis of Duchenne muscular dystrophy. *Mol. Cell. Biol. Hum. Dis. Ser. Rev.* **3**, 139-166.

Goto, T., Davidson, L., Asashima, M. and Keller, R. (2005). Planar cell polarity genes regulate polarized extracellular matrix deposition during frog gastrulation. *Curr. Biol.* **15**, 787-793.

Hardcastle, Z. and Papalopulu, N. (2000). Distinct effects of XBF-1 in regulating the cell cycle inhibitor p27 (XIC1) and imparting a neural fate. *Development* **127**, 1303-1314.

Harland, R. M. (1991). In situ hybridization: an improved whole-mount method for Xenopus embryos. *Methods Cell Biol.* **36**, 685-695.

Hidalgo, M., Sirour, C., Bello, V., Moreau, N., Beaudry, M. and Darribère, T. (2009). *In vivo* analyzes of dystroglycan function during somitogenesis in *Xenopus laevis*. *Dev. Dyn.* **238**, 1332-1345.

Ibraghimov-Beskrovnaya, O., Ervasti, J. M., Leveille, C. J., Slaughter, C. A., Sernett, S. W. and Campbell, K. P. (1992). Primary structure of dystrophin-associated glycoproteins linking dystrophin to the extracellular matrix. *Nature* **355**, 696-702.

Ilsley, J. L., Sudol, M. and Winder, S. J. (2001). The interaction of dystrophin with beta-dystroglycan is regulated by tyrosine phosphorylation. *Cell Signal.* **13**, 625-632.

Keller, R., Cooper, M. S., Danilchik, M., Tibbetts, P. and Wilson, P. A. (1989). Cell intercalation during notochord development in *Xenopus laevis*. *J. Exp. Zoolog.* **251**, 134-154.

Lunardi, A. and Dente, L. (2002). Molecular cloning and expression analysis of dystroglycan during *Xenopus laevis* embryogenesis. *Mech. Dev.* **119 Suppl. 1**, S49-S54.

Moore, J. C. and Winder, S. J. (2010). Dystroglycan versality in cell adhesion: a tale of multiple motifs. *Cell Commun. Signal.* **8**, 3.

Moreau, N., Alfandari, D., Gaultier, A., Cousin, H. and Darribère, T. (2003). Cloning and expression patterns of dystroglycan during the early development of *Xenopus laevis*. *Dev. Genes Evol.* **213**, 355-359.

Nieuwkoop, P. D. and Faber, J. (1994). *Normal Table of Xenopus Laevis*. New York: Garland Publishing.

Parsons, M. J., Pollard, S. M., Saude, L., Feldman, B., Coutinho, P., Hirst, E. M. and Stemple, D. L. (2002a). Zebrafish mutants identify an essential role for laminins in notochord formation. *Development* **129**, 3137-3146.

Parsons, M. J., Campos, I., Hirst, M. A. E. and Stemple, D. L. (2002b). Removal of dystroglycan causes severe muscular dystrophy in zebrafish embryos. *Development* **129**, 3505-3512.

Philippe, M., Léger, T., Desvaux, R. and Walch, L. (2013). Discs Large 1 (Dlg1) scaffolding protein participates with clathrin and adaptator protein complex 1 (AP-1) in forming Weibel-Palade Bodies of endothelial cells. *J. Biol. Chem.* **288**, 13046-13056.

Development (2014) 141, 4569-4579 doi:10.1242/dev.116103

Rodriguez, O. C., Schaefer, A. W., Mandato, C. A., Forscher, P., Bement, W. M. and Waterman-Storer, C. M. (2003). Conserved microtubule-actin interactions in cell movement and morphogenesis. *Nat. Cell Biol.* **5**, 599-609.

Rolo, A., Skoglund, P. and Keller, R. (2009). Morphogenetic movements driving neural tube closure in Xenopus require myosin IIB. *Dev. Biol.* **327**, 327-338.

Rozario, T., Dzamba, B., Weber, G. F., Davidson, L. A. and DeSimone, D. W. (2009). The physical state of fibronectin matrix differentially regulates morphogenetic movements *in vivo*. *Dev. Biol.* **327**, 386-398.

Sirour, C., Hidalgo, M., Bello, V., Buisson, N., Darribère, T. and Moreau, N. (2011). Dystroglycan is involved in skin morphogenesis downstream of the Notch signaling pathway. *Mol. Biol. Cell* **22**, 2957-2969.

Skoglund, P. and Keller, R. (2007). Xenopus fibrillin regulates directed convergence and extension. *Dev. Biol.* **301**, 404-416.

Skoglund, P., Dzamba, B., Coffman, C. R., Harris, W. A. and Keller, R. (2006). Xenopus fibrillin is expressed in the organizer and is the earliest component of matrix at the developing notochord-somite boundary. *Dev. Dyn.* **235**, 1974-1983.

Skoglund, P., Rolo, A., Chen, X., Gumbiner, B. M. and Keller, R. (2008). Convergence and extension at gastrulation require a myosin IIB-dependent cortical actin network. *Development* **135**, 2435-2444.

Sotgia, F., Lee, H., Bedford, M. T., Petrucci, T., Sudol, M. and Lisanti, M. P. (2001). Tyrosine phosphorylation of beta-dystroglycan at its WW domain binding motif, PPxY, recruits SH2 domain containing proteins. *Biochemistry* **40**, 14585-14592.

Sotgia, F., Bonuccelli, G., Bedford, M., Brancaccio, A., Mayer, U., Wilson, M. T., Campos-Gonzalez, R., Brooks, J. W., Sudol, M. and Lisanti, M. P. (2003). Localization of phospho-beta-dystroglycan (pY892) to an intracellular vesicular compartment in cultured cells and skeletal muscle fibers *in vivo*. *Biochemistry* **42**, 7110-7123.

Spence, H. J., Chen, Y.-J., Batchelor, C. L., Higginson, J. R., Suila, H., Carpen, O. and Winder, S. J. (2004). Ezrin-dependent regulation of the actin cytoskeleton by beta-dystroglycan. *Hum. Mol. Genet.* **13**, 1657-1668.

Veeman, M. T., Nakatani, Y., Hendrickson, C., Ericson, V., Lin, C. and Smith, W. C. (2008). Chongmague reveals an essential role for laminin-mediated boundary formation in chordate convergence and extension movements. *Development* **135**, 33-41.

Vicente-Manzanares, M., Ma, X., Adelstein, R.S. and Horwitz, A. R. (2009). Non-muscle myosin II takes centre stage in cell adhesion and migration. *Nat. Rev. Mol. Cell Biol.* **10**, 778-790.

Williamson, R. A., Henry, M. D., Daniels, H. J., Hrstka, R. F., Lee, J. C., Sunada, Y., Ibraghimov-Beskrovnaya, O. and Campbell, K. P. (1997). Dystroglycan is essential for early embryonic development: disruption of the Reichert's membrane in Dag1-null mice. *Hum. Mol. Genet.* **6**, 831-841.

Yatsenko, A. S., Kucherenko, M. M., Pantoja, M., Fischer, K. A., Madeoy, J., Deng, W. M., Schneider, M., Baumgartner, S., Akey, J., Shcherbata, H. R. et al. (2009). The conserved WW-domain binding sites in Dystroglycan C-terminus are essential but partially redundant for Dystroglycan function. *Dev. Biol.* **9**, 18-27.